Development of Quicklook Processor for Circularly Polarized Synthetic Aperture Radar onboard GAIA-II Microsatellite

Bambang Setiadi[†‡], Zafri Baharuddin[†], Good Fried Panggabean[†], Hiroaki Kuze[†], and J.T. Sri Sumantyo[†]
[†]Center for Environmental Remote Sensing ChibaUniversity, Chiba, Japan
[‡]Research Center for Geotechnology, Indonesian Institute of Sciences, Bandung, Indonesia

***Abstract*—**Synthetic Aperture Radar sensor produce large amount of raw data and requires high amount of computing resources to process the data into full resolution image. Although most SAR application requires high-resolution image, there are cases where low-resolution is also important, for example when browsing from large collection of raw data to find the area of interest. A quick-look SAR processor for L-band Circularly Polarized Synthetic Aperture radar sensor onboard GAIA-II microsatellite is developed to produce low-resolution images and enable rapid preview of CP-SAR images on commodity of the shelf computer system. The algorithm is based on modified spectral analysis (SPECAN) algorithm for SAR image formation. The result is validated using actual raw data from JERS-1 SAR sensor that has similar characteristics with GAIA-II CP SAR sensor.

***Keywords*—**SAR processing, quick-look, modified SPECAN algorithm, circularly polarized SAR, GAIA II.

I. Introduction

SYNTHETIC Aperture Radar (SAR) is a well-known remote sensing technology that offers the possibility of earth observation under all weather conditions with day- and nighttime operation [1]. It provides high resolutions images for various applications such as: geoscience and climate change research, environmental and Earth system monitoring, 2D, 3D and 4D mapping, change detection, security-related applications up to planetary exploration [2].

Most of SAR sensors for earth remote sensing applications available today are linear polarized sensors, which send and receive horizontal or vertical microwave (HH, VV, HV and VH). Josaphat Microwave Remote Sensing Laboratory (JMRSL) of Chiba University has been working on the development of a Circularly Polarized SAR (CP-SAR) sensor to explore the usage of elliptical polarization wave for SAR applications. The objective of using elliptical polarization wave is to explore various possibilities offered by circularly polarized scattering phenomena. **Table 1** summarizes various basic experiments and applications of CP-SAR [3].

Corresponding author: J.T.S.Sumantyo (email: jtetukoss@faculty.chiba-u.jp).
This paper was submitted on December 6, 2015; revised on December 20, 2015; and accepted on December 27, 2015.

Table I CP-SAR Objectives

Field	Item	Details
Basic SAR Experiments	Scattering mechanism of CP microwave	• Studying scattering mechanism from vegetation, cryosphere, soil and rocks, desert, etc.
	Interferometry	• Linear versus circular polarization interferometric SAR • DEM extraction using CP wave
	Axial ratio image	• Vegetation, geologic, cryosphere mapping using axial ratio image
SAR Applications	Land cover mapping	• Forest/non-forest area classification • Paddy field/wet land extraction • Mangrove area mapping • Snow - iceberg detection
	Disaster monitoring	• Earthquake • Volcano eruption • Flood, forest fire, landslide, etc.
	Cryosphere monitoring	• Iceberg, glacier, • Arctic routing
	Ocean monitoring	• Oil spill • Ocean wave monitoring

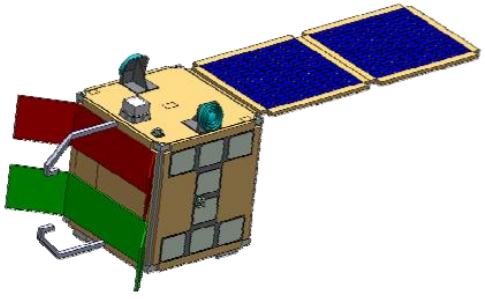

Figure 1 CP-SAR sensor onboard GAIA-II microsatellite

As part of the development roadmap, JMRSL plan to deploy the L-band CP-SAR sensors on airborne and spaceborne platform [4]. The airborne platform will use an unmanned aerial vehicle (UAV) named JX-2 and the spaceborne platform will be a microsatellite called GAIA-II. An illustration of the CP-SAR onboard the microsatellite is depicted in **Figure 1**.

CP-SAR sensor is utilizing the elliptical wave propagation and scattering phenomenon by radiating and receiving the elliptically polarized wave, which includes circular and linear polarizations. Elliptical polarized sensor is considered not depend on the platform posture, and able to lower the effect of Faraday rotation in Ionosphere [4]. The sensor transmits and receives L-band chirp pulses with PRF between 2,000 to 2,500 Hz. It is designed as a low cost, light, low power, low profile sensor that transmits and receives left-handed circular polarization (LHCP) and right-handed circular polarization (RHCP). Besides producing single look complex (SLC) image and amplitude image, this sensor can also generate various SAR images unique to elliptically polarized sensor e.g. axial ratio image (ARI), ellipticity and tilt angle.

GAIA-II satellite will orbit between 500 to 700 km, with 50 km swath width and maximum spatial resolution of 30 m. The L-band (1.27 GHz) antenna size is 2.0 m in elevation and 5.0 in azimuth direction, with 97.6° inclination angle and 29.0° off nadir angle. The satellite has the form of 1m cube with maximum weight of 100 kg. **TABLE II** summarizes the specification of CP-SAR onboard GAIA-II [3].

TABLE II CP SAR SENSOR ONBOARD GAIA II SPECIFICATION

Parameter	Value
Altitude	500-700 km
Inclination angle	97.6°
Frequency	1.27 GHz
Polarization	LL, LR, RL, RR
Gain/Axial ratio	>30 dBic / < 3 dB
Off nadir angle	29°
Swath width	50 km
Spatial resolution	30 m
Peak power	90-300 W
Bandwidth	10 MHz
PRF	2000-2500 Hz
Platform size	1 m × 1 m × 1 m
Weight	100 kg
Antenna size	2.0 m × 5.0 m

Besides the radar subsystem that transmits and receives signals, another important component of a SAR system is the processor subsystem that converts phase histories signal or SAR raw data into images. Various SAR image formation algorithms are available nowadays and some of the most commonly used are: Range Doppler, Chirp Scaling and Omega-K [5]. This image formation subsystem is commonly known as SAR signal processor or SAR processor.

SAR sensor produces large amount of raw data during data acquisition operation and the processing of those data into high-resolution image requires high amount of computing power and memory. Although most SAR application requires high-resolution image, there are cases where low-resolution is needed. As an example, when a user has to browse from large collection of raw data in order to find the suitable scene containing the region of interest. Another possible scenario is when rapid response to disaster or emergency situation needs quick overview of a specific geographic area.

Images in preview process do not have to be in high resolution, thus a quick-look processor for generating medium to low-resolution image is necessary. Several quick-look processor for airborne and space borne system has been developed around the world [6,7,8,9,10].

A feasible quick-look SAR processor is presented for L-band CP-SAR onboard GAIA-II microsatellite currently under development. It is developed to produce low-resolution images and enable rapid preview of CP-SAR images on commodity of the shelf computer system. Both the algorithm and its software implementation are discussed. The algorithm is based on modified spectral analysis (SPECAN) algorithm for SAR image formation [5]. The result is validated using actual raw data from JERS SAR sensor that has similar characteristics with GAIA-II CP-SAR sensor.

II. CP-SAR SYSTEM ONBOARD GAIA II SATELLITE

A functional block diagram of the CP-SAR system onboard GAIA II satellite and SAR processor on the ground station is shown in **Figure 2**. The CP-SAR sensor system onboard GAIA II satellite is composed of a chirp signal generator, RF Module, CP SAR antenna, analog to digital converter and data recorder, motion sensing module and data downlink module. The data downlink module will transmit received SAR signal to the ground station via data link antenna. The CP antenna is connected to the RF module, while the motion sensing module contains an inertial measurement unit (IMU) that receives position signals from GPS antenna. In order to communicate with the ground station, a data link antenna is connected to the data downlink module.

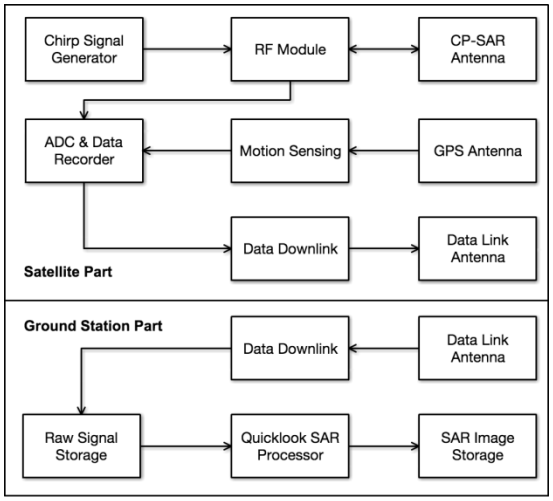

Figure 2 CP-SAR functional block diagram

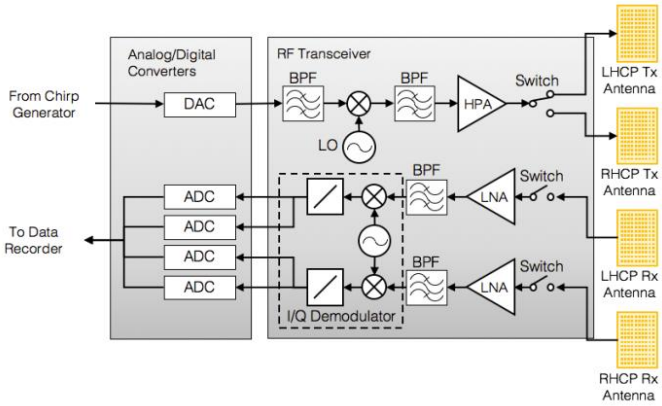

Figure 3 Block diagram of RF and CP antenna

The RF subsystem consists of a transmitter, receiver, local oscillator and low noise amplifier weights approximately 10 kg. The transmitter mixes the 150 MHz bandwidth chirp up to 1.27 GHz for transmission. The receiver and local oscillator are used to mix the RF radar return from the antenna to an offset baseband and amplify it so that it can be sampled by the ADC subsystem. **Figure 3** shows the block diagram of RF and CP antenna subsystem.

The main objective of quicklook processor for CP-SAR sensor onboard GAIA-II satellite is to convert the received signals into a low or medium resolution SAR image. While SAR processing is a highly intensive computational process, the trade-off between processing speed and image quality becomes a major concern. Since our objective is to get a preview of SAR images during a mission in shortest time possible, the processing speed has higher priority than image quality.

In terms of SAR signal processing, the algorithm to produce amplitude image from linear and circular polarized sensor is similar because polarization information is not used. In actual operation, CP-SAR sensor will operate in full polarimetric mode: LL, LR, RL and RR polarization which can be divided into four channel ADC output. The quicklook processor will produce an amplitude image for each polarization. **Figure 6** shows the general flow of data processing done by the CP-SAR processor subsystem.

In general, the quicklook processing subsystem consists of a file processor loop that reads raw signal and motion data file from the data recording subsystem transmitted by the Data Downlink module. The processor converts the raw signal using quicklook algorithm and writes the resulting image to the storage. The processed SAR images in data recorder then can be transmitted to the ground system via the data downlink in order to give a quick preview of the currently observed SAR area.

The chirp signal generator subsystem generates chirp signal as the input for RF subsystem. It is implemented using a field programmable gate array (FPGA) to enable rapid modification to the generated chirp signal according to the platform condition. The chirp signal generator must be able to produce chirp signal with various configurations depending on the mission requirement such as flight height and platform speed. The parameters of generated chirp signal that can be modified are: chirp bandwidth, pulse duration and pulse repetition frequency (PRF). Direct digital synthesizer (DDS) technique is used for the chirp signal generation process because it has many advantages compare to its analog counterpart. **Figure 4** shows an example of real and imaginary components of the chirp signal created by the signal generator subsystem displayed on spectrum analyzer [5].

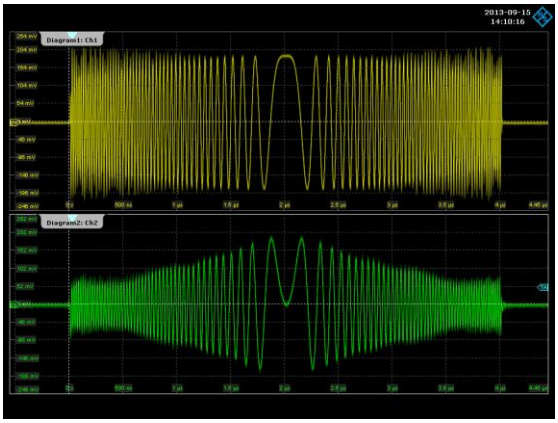

Figure 4 Real and imaginary part of the chirp signal waveform from signal generator

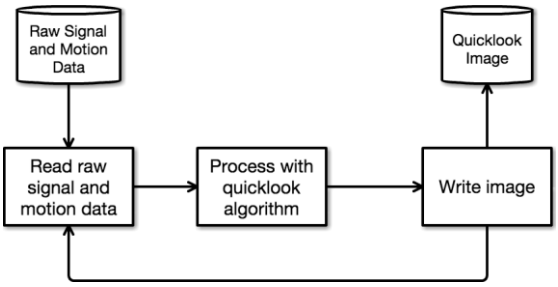

Figure 5 Real and imaginary part of chirp signal waveform

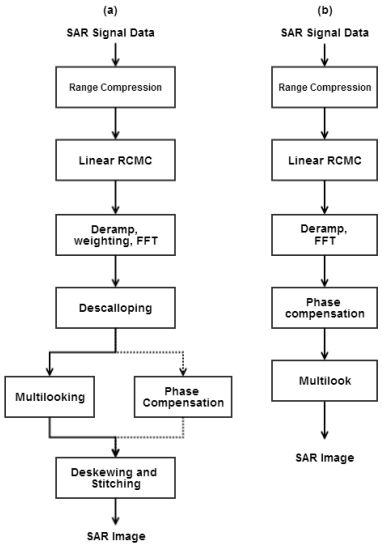

Figure 6 SPECAN algorithm processing flow: (a) Reference SPECAN algorithm, (b) implemented modified SPECAN algorithm

The analog to digital converter/data recorder subsystem handles the sampling and down-converting of signal received by the CP antenna. After down-converting to the baseband, the data are stored in solid-state drive storage inside the data recorder. There is a random access memory between solid-state drive storage and the four ADC module functioning as a buffer before signal is written to the solid-state drive. This data is known as a raw SAR data or phase histories, and will be processed further using signal processing technique in order to produce a SAR image.

III. Modified SPECAN Algorithm

The original SPECAN algorithm depicted in **Figure 6(a)** consists of general processing in range and azimuth direction [5]. Range processing contains only pulse compression of received signals in the range direction, while azimuth processing consists of linear range cell migration correction (RCMC), deramping with weighting and FFT, descalloping, multilooking or phase compensation and deskewing with stitching operation. The range compression is done by pulse compression between the received signals in a range bin with the replica of transmitted signal. Using fast convolution technique, the range compression is carried out as multiplication in the frequency domain involving FFT and inverse FFT operation.

The azimuth processing steps are started with a linear RCMC operation to compensate the effect of range migration. After deramping and FFT operation that equals to time domain convolution, a descalloping operation takes place. Descalloping is done by applying functions which are inversely proportional to the predicted antenna gain pattern function to correct the scalloping effect due to different magnitude of each burst. If required, multilook processing must be done to generate a multilook image, but in the case of single look image, only phase compensation is done instead. The last stage is the step to correct the skewing effect in the result of each burst and a stitching process to combine all of the resulting SAR images into a single look image.

Figure 6(b) shows the flow of modified SPECAN algorithm implemented in this work. The modified algorithm consists only of range compression, linear RCMC, deramping and FFT, phase compensation and multilook process. Range compression is implemented as an FFT operation to range samples in an azimuth gates with a range reference function, followed by multiplication operation and an IFFT operation on the result. A single range reference function is used for all azimuth gates. After range compression, RCMC is applied by shifting the range compressed data set at certain value for each range gates. First the range curvature is calculated using Doppler centroid, chirp rate and chirp center value, followed by interpolation operation. The calculation is executed in the frequency domain, by applying a pair of FFT and inverse FFT operation.

Deramping calculation consists of a creation of complex matched filter using Doppler and PRF information, followed by matched filtering operation to the data set in range gates. Deramping is based on the stretch technique which allows linear manipulation of the time and bandwidth coordinates of a linear frequency modulated signal by mixing it with another signal of different frequency-time slope to slow down, speed up or time reverse the signal [18,19].

Assuming that a linear frequency modulation (FM) signal has the following form:

$$s(\mathrm{t}) = e^{j\pi K(t-\tau_c)^2} \qquad -\frac{T_c}{2} \le \mathrm{t} \le \frac{\mathrm{T_c}}{2}, \tag{1}$$

where K is the signal FM rate, T_c is pulse time extent, and τ_c is the time position of the zero frequency of the signal. The zero frequency of the target is the static phase point, the time at which the phase rate goes from positive to negative or vice versa. If the phase switch-over occurs in the middle of the signal time duration, the zero frequency will be at the same position as the center frequency.

The instantaneous frequency of the FM signal can be calculated using the first derivative of its phase, θ. From Equation 1, the phase, $\theta_s(t)$, of the signal is:

$$\theta_s(t) = \pi K(t-\tau_c)^2$$
$$\omega_{inst}(t) = \frac{d\theta_s(t)}{dt} = 2\pi K(t-\tau_c), \tag{2}$$

which shows that the instantaneous frequency, $\omega_{inst}(t)$, is a linear function of time, t.

Next, we apply the stretch technique. If the linear FM signal in Equation (1) is multiplied with another linear FM signal $s_1(t)$ with different FM rate $K_1(t)$, and shifted with respect to $s(t)$, the product is a linear FM signal with FM rate equals to $(K+K_1)$:

$$s_1(t) = e^{j\pi K_1(t-\tau_r)^2} \qquad -\frac{T_c}{2} \le t \le \frac{T_c}{2},$$
$$s(t)s_1(t) = e^{j\pi(K+K_1)t^2} e^{-j\pi K_1(K\tau_c+K_1\tau_r)t} e^{j\pi\left(K\tau_c^2+K_1\tau_r^2\right)t} \tag{3}$$

The first term in Equation (3) is a linear FM signal with the FM rate of $(K+K_1)$, the second term is a constant frequency signal, and the third is a constant complex number.

In SPECAN algorithm, the same linear FM signal multiplication technique is also applied. The target signal is transformed from linear FM chirps to constant frequency signal using $-K$ as the value of K_1. This process creates a deramped signal, $d(t)$, such as

$$d(t) = e^{2j\pi K(\tau_r-\tau_c)t}\, e^{j\pi K\left(\tau_r^2-\tau_c^2\right)^2} \qquad -\frac{T_c}{2} \le t \le \frac{T_c}{2} \tag{4}$$

The phase, $\theta_d(t)$, and instantaneous frequency, $\omega'_{inst}(t)$, of this signal are

$$\theta_d(t) = \pi K[2(\tau_r-\tau_c)t + (\tau_c^2-\tau_r^2)]$$
$$\omega'_{inst}(t) = 2\pi K(\tau_r-\tau_c), \tag{5}$$

where the instantaneous frequency does not vary with time.

In SPECAN algorithm, the matched filter is created using the FM rate of the transmitted pulse to generate the conjugate of the ideal received signal. It is then used to deramp the received data by a complex multiplication in the time domain. After deramping, each target will have a constant frequency value proportional to the time position of its zero Doppler frequency with respect to that of the reference function in Equation (2).

To narrow most of the energy of each target to a single frequency bin, a FFT operation is performed on this signal. The relative positions of the targets' time locations will be detected at the correct positions relative to each other. Short length FFT blocks are placed along the deramped signal such that each target's trajectory is included in at least one FFT input vector [10].

Several important issues related to FFT operation after the deramping are: how to determine the position of the first FFT, how to calculate the length of FFT, how to select the correct FFT output, and where to put subsequent FFT operation. The length of the FFT operation is influenced by several factors such as the desired azimuth resolution, prevention of aliasing and computing efficiency [10]. Larger number of FFT point will cause heavier computational load.

The azimuth resolution obtained by an N_{FFT} point of FFT can be formulated as

$$\rho_{az-CP} = \left(\frac{0.886\ PRF\ \gamma_{w,az}}{N_{FFT}K_a}\right) vcos\ \theta_{sq}, \qquad (6)$$

where $\gamma_{w,az}$ is the broadening factor of the weighting window, K_a is the azimuth FM rate, and θ_{sq} is the squint angle which in our case equals to 0. The length of FFT is governed by the PRF time: a mixed target will happen if it is longer than the PRF time. Therefore, the upper limit of the FFT length is the PRF value.

The output sample spacing of the FFT output is calculated as one PRF in the frequency domain, which equals to PRF/N_{FFT} in frequency units: in time units, this corresponds to

$$\Delta_y = \frac{PRF}{N_{FFT}K_a}. \qquad (7)$$

If the FFT size is not an efficient length (i.e., not in the power of 2), the value can be zero padded to a nearest better length. After this operation, the number of good points in the FFT output (N_{good}) can be calculated as

$$N_{good} = N_{FFT}\left(T_a - \frac{N_{FFT}}{PRF}\right)\frac{K_a}{PRF} \qquad (8)$$

where T_a is the synthetic exposure time. The frequency of target after deramping (f_{tar_dr}) can be given as

$$f_{tar\_dr} = f_{\eta_c} + K_a(\eta'_{mid} - \eta'_{ramp_0}), \qquad (9)$$

where f_{η_c} is the Doppler centroid frequency, η'_{mid} is time at the middle of target exposure, and η'_{ramp_0} is the time at which the reference function passes through zero frequency. Then, the position of the good FFT can be calculated by

$$k = \frac{N_{FFT}}{PRF} f_{tar\_dr} + 1. \qquad (10)$$

This indicates that the deramped frequency $(k-1)\ PRF/N_{FFT}$ is at the k-th element, where the value k is between 1 and N_{FFT}.

After the valid pixel number is calculated, valid pixel value determines the size of final result of phase compensation. The phase compensation of azimuth deramped signal is done in the frequency domain. The phase compensation process is composed of FFT operation, filter calculation, and matched filtering operation between the filter and the range gate of the deramped signal dataset. Phase compensation also includes interpolation operation depending on the calculated image resolution. In the modified SPECAN algorithm, the descalloping process is skipped in order to avoid interpolation operation to reduce computation load.

The last step of this quicklook processing is multilooking which will reduce the scalloping effect in the image. Multilooking process is carried out by averaging different parts of the signal spectrum to form processed SAR images.

TABLE IV SCENE PARAMETERS

Parameter	Value
Satellite	JERS-1
Wavelength	23.5 cm
Polarization	HH
Path/Row/Orbit	91/315/32456
Observation date	98/ 1/17
Off-nadir angle	34.90 deg.
PRF	1555.20 Hz
Pulse length	35.00 μs
Sampling Window Start Time	4.613028×10^{-3} s
Sampling Rate	1.707600×10^{7} Hz
Satellite time	9.941828×10^{3} s
Total scene size	6144 × 19904 (range × azimuth)

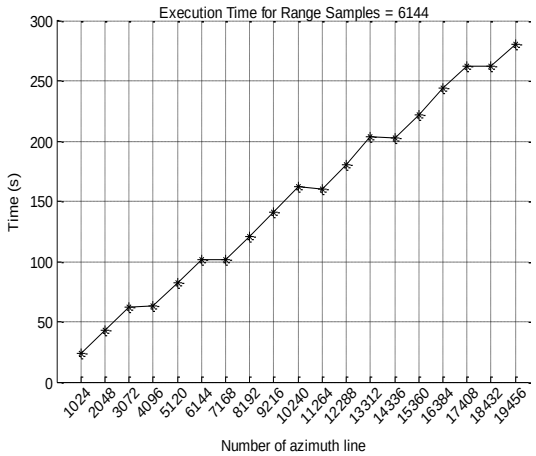

Figure 7 Processing speed of a single look with different number of azimuth line

IV. EXPERIMENT AND RESULT

Since actual data from the CP-SAR sensor is not yet available, the functionality of the quicklook processor is tested using raw data from JERS-1 SAR sensor. JERS-1 SAR has

been chosen because it has the same wavelength with the currently developed CP-SAR system and the operating orbit of the satellite is similar with the future GAIA II. The selected raw data set represents an area of approximately 75 km × 75 km, acquired over southern part of Bali Island, Indonesia.

A test has been performed in order to compare the processing speed of the quicklook processor against various numbers of processed samples in azimuth direction. In order to show the quality degradation, first a high quality image obtained from the same scene and processed using the conventional range-Doppler algorithm is shown in **Figure 8(a)**. **Figure 8(b)** shows the same scene processed using the algorithm proposed in section III.

The GAIA II quicklook processor has been developed using C programming language, compiled with GNU C compiler and work in a single thread for execution. The scene presented here has been generated on on a 2 GHz Quad Core Intel Xeon 5130 CPU hardware with 12 GB of RAM.

Evaluation on the processing time for various numbers of azimuth lines is shown in **Figure 7**. The processing uses the same number of samples in the range direction but with increasing number of azimuth lines. The range samples used is 6144 in order to cover the whole samples in the range direction. The graph shows that the processing time increases linearly with the number of azimuth lines processed.

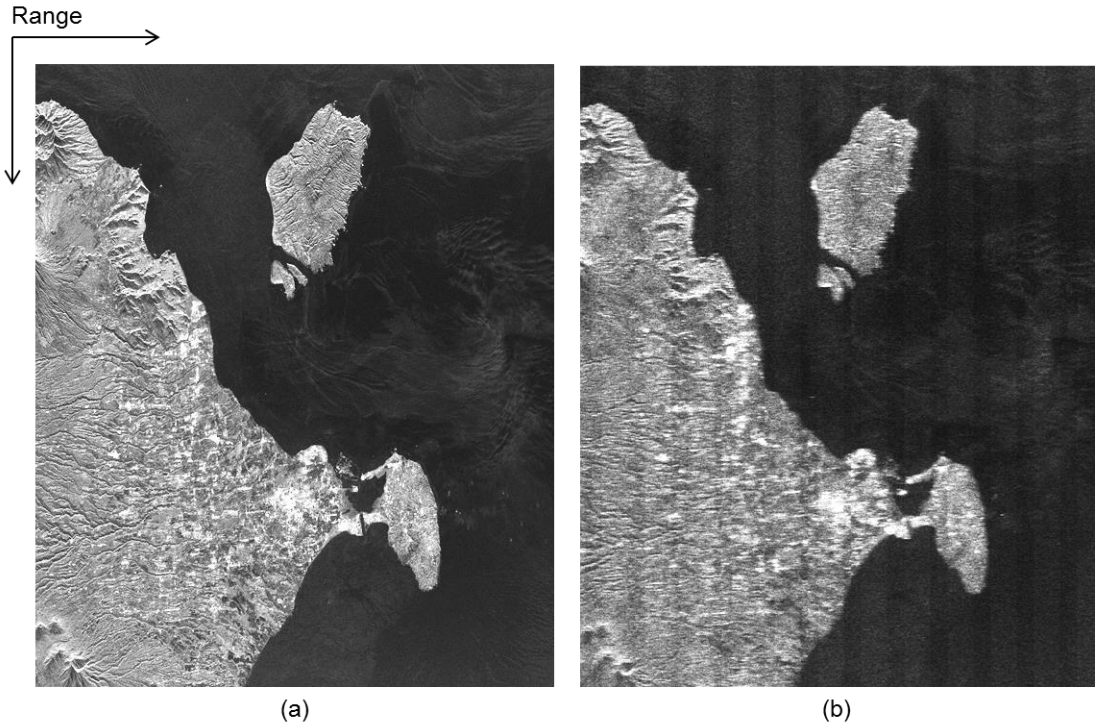

Figure 8 Amplitude image of Bali island processed with (a) the range-Doppler algorithm, and (b) modified SPECAN algorithm. The horizontal axis represents range direction. Resolution degradation and scalloping effect are clearly shown in (b)

V. Conclusion

The development of quicklook processor for CP-SAR sensor onboard GAIA-II microsatellite has been presented in this paper. The processor used modified SPECAN algorithm. The imaging capability is tested using JERS-1 raw SAR data which is an L-band satellite-borne sensor with similar specification. Using commodity of the shelf computer system, the processor is able to produce low resolution image for browsing from a large collection of raw data. The system is able to present user lower resolution quicklook image faster than using the original RDA algorithm, which is suitable in the case where a rapid lower resolution SAR image production is critical such as in the case of disaster related emergency or where the user needs to be able to browse and select images containing area of interest from a large collection of raw SAR data.

VI. Future Works

In order to prepare the processor towards the actual CP SAR sensor data, instead of using raw data from different sensor with closely similar specification, a raw data simulator that can produce simulated data with precise system specification is needed. The raw data simulator can be used to overcome the differences in several core system parameters such as sampling rate, PRF, sampling window start time. The simulated data can also be used to measure the image quality produced by the quicklook processor. Further work also needed to make the processor run faster by taking the advantage of parallel processing available on multicore CPU and many-core GPU hardware ubiquitously available on commodity of the shelf computer system.

ACKNOWLEDGMENT

This research was supported by Chiba University; the Japan Society for the Promotion of Science (JSPS); the National Institute of Information and Communication Technology (NICT) for International Research Collaboration Research Grant; Chiba University COE Start-up Programme; the Japanese Ministry of Education and Technology (Monbukagakusho); Japan International Cooperation Agency (JICA), Japan Science and Technology Agency (JST), Weathernews, PASCO and JAMSS.

REFERENCES

[1] Skolnik, M. Radar Handbook, Third Edition; Skolnik, M., Ed.; Third.; McGraw-Hill Professional, 2008; p. 1328.

[2] A. Moreira, P. Prats-Iraola, M. Younis, G. Krieger, I. Hajnsek and K. P. Papathanassiou "A tutorial on synthetic aperture radar", IEEE Geosci. Remote Sens. Mag., vol. 1, no. 1, pp.6 -43

[3] Sri Sumantyo, J. T. Circularly Polarized Synthetic Aperture Radar Onboard Unmanned Aerial Vehicle (CP-SAR UAV). In Autonomous Control Systems and Vehicles; Nonami, K.; Kartidjo, M.; Yoon, K.-J.; Budiyono, A., Eds.; Springer Japan, 2013; pp. 175–192. CrossRef

[4] J. T. S. Sumantyo, "Progress on development of synthetic aperture radar onboard UAV and microsatellite," in 2014 IEEE Geoscience and Remote Sensing Symposium, 2014, pp. 1081–1084. CrossRef

[5] Cumming, I.; Wong, F.: Digital Processing of SAR Data, Artech House, Norwood, 2005

[6] Dall J., Jorgensen J.H., Christensen E.L., and Madsen S.N. "Real-time processor for the Danish airborne SAR. IEE Proceedings-F, Vol 139, No 2 , April 1992

[7] Moreira A. "Real-Time Synthetic Aperture Radar (SAR) with a New Subaperture Approach". IEEE Trans on Geo- science and Remote Sensing Vol 30, No 4, July 1992, pp 714- 722.

[8] Gustavsson A., Frolind P.O., Hellsten H., Jonsson T., Larsson B., and Stenstrom G. "The Airborne VHF SAR System Carabas," in IGARSS '93, Vol 11, pp 558-562.

[9] L. Xiaoqin, W. Yirong, and P. Hailiang, "Quicklook processing for RADARSAT data," in IGARSS 2000. IEEE International Geoscience and Remote Sensing Symposium., 2000, vol. 5, pp. 2281–2283. CrossRef

[10] Hobooti, H. Radiometric correction in range-SPECAN SAR processing, University of British Columbia, 1995, p. 117.